

GA-A23351

**ELECTROMAGNETIC EFFECTS ON PLASMA
MICROTURBULENCE AND TRANSPORT**

by
P.B. SNYDER and G.W. HAMMETT

APRIL 2000

DISCLAIMER

This report was prepared as an account of work sponsored by an agency of the United States Government. Neither the United States Government nor any agency thereof, nor any of their employees, makes any warranty, express or implied, or assumes any legal liability or responsibility for the accuracy, completeness, or usefulness of any information, apparatus, product, or process disclosed, or represents that its use would not infringe privately owned rights. Reference herein to any specific commercial product, process, or service by trade name, trademark, manufacturer, or otherwise, does not necessarily constitute or imply its endorsement, recommendation, or favoring by the United States Government or any agency thereof. The views and opinions of authors expressed herein do not necessarily state or reflect those of the United States Government or any agency thereof.

ELECTROMAGNETIC EFFECTS ON PLASMA MICROTURBULENCE AND TRANSPORT

by
P.B. SNYDER and G.W. HAMMETT*

This is a preprint of a paper submitted for
publication in *Phys. Rev. Lett.*

*Princeton Plasma Physics Laboratory, Princeton, New Jersey.

Work supported by
the U.S. Department of Energy under
Grant No. DE-FG03-95ER54309,
Contract No. DE-AC02-76CG03073, and NSF fellowship

**GA PROJECT 03726
APRIL 2000**

Electromagnetic Effects on Plasma Microturbulence and Transport

P. B. Snyder

General Atomics, P.O. Box 85608, San Diego, California 92186-5608

G. W. Hammett

Princeton Plasma Physics Laboratory, Princeton, New Jersey 08543

Abstract

Results are presented from three dimensional kinetic-fluid simulations of pressure gradient driven microturbulence using a new, numerically efficient model which includes self-consistent magnetic fluctuations and non-adiabatic electron dynamics. A transition from electrostatic ion-drift turbulence to Alfvénic turbulence is seen at modest values of the plasma pressure. Significant electromagnetic effects on heat conductivity are observed, including a dramatic increase as the ideal ballooning threshold is approached, particularly when electron Landau damping is included. Turbulent spectra show a number of similarities to experimental fluctuation measurements.

52.25.Fi, 52.30.Jb, 52.35.Ra, 52.55.Fa

A quantitative physical understanding of turbulent transport in magnetized plasmas is crucial to the analysis of present experiments and the design of future fusion devices. Therefore, substantial effort has been invested in the development of increasingly realistic numerical simulations of plasma turbulence in the hot interior of fusion relevant plasmas [1–6]. These simulations employ analytic techniques which reduce the dimensionality of the phase space, and which remove many of the widely disparate spatial and temporal physical scales characteristic of magnetized, collisionless plasma [7–10]. Past simulations have led to rapidly expanding understanding of plasma turbulence and transport, though limitations remain. In core turbulence simulations, fluctuations have generally been assumed to be purely electrostatic. However, magnetic fluctuations can both alter the dynamics of primarily electrostatic instabilities such as the ion temperature gradient mode (ITG), and introduce electromagnetic instabilities such as the kinetic ballooning mode (KBM), the kinetic analog of the ideal ballooning mode. Furthermore, the electrostatic approximation requires not only that the ratio of plasma to magnetic pressure (β) be small, but also that β be far below the ideal magnetohydrodynamic (MHD) critical β_c for linear instability [11]. Hence this approximation can be expected to break down both in the interior of a high β plasma, and in any region where pressure gradients are sharp enough to push the plasma close to ideal instability, as often occurs in core transport barriers and in the edge region.

Interesting fluid simulations of the collisional outer edge region have demonstrated that self-consistent magnetic fluctuations are critical for prediction of edge transport [12–15]. This, along with the likelihood that an attractive fusion device would have both high interior β and interior transport barriers, strongly motivates the development of a practical model for core turbulence including magnetic fluctuations. In the hot plasma core, the collisional fluid methods often used in the edge region are not valid. Furthermore, the wide separation between the fast electron transit timescale and the slower ion drift and Alfvénic turbulence timescales makes direct simulation via kinetic, gyrokinetic, or gyrofluid methods challenging. Most previous core simulations have assumed electrostatic fields and adiabatic passing electrons in order to avoid explicitly treating electron dynamics along the field.

Electromagnetic simulations must include passing electron dynamics along the field because electrons carry the dominant current perturbations which drive magnetic fluctuations. Here we develop a method which employs an expansion in the electron to ion mass ratio, allowing for practical simulations of core turbulence including self-consistent electromagnetic fluctuations and non-adiabatic passing electron dynamics.

Electron equations are derived by taking velocity space moments of the drift kinetic equation. Fluctuating quantities are taken to have length and time scales characteristic of ion drift waves, or, equivalent in this ordering, shear Alfvén waves. A formal expansion in the electron to ion mass ratio, keeping the lowest order terms and those that are smaller by $\mathcal{O}(\sqrt{m_e/m_i})$, leads to the moment hierarchy,

$$\frac{\partial n}{\partial t} + \mathbf{v}_E \cdot \nabla n + B \tilde{\nabla}_{\parallel} \frac{u_{\parallel}}{B} + i\omega_* \phi + i\omega_d (\phi - n - T^{(0)} - T_{\perp}^{(1)}/2 - T_{\parallel}^{(1)}/2) = 0 \quad , \quad (1)$$

$$\frac{\partial A_{\parallel}}{\partial t} + \tilde{\nabla}_{\parallel} (\phi - n - T^{(0)} - T_{\parallel}^{(1)}) + (1 + \eta_e) i\omega_* A_{\parallel} = \mathcal{C}_{ei} \quad . \quad (2)$$

Here \mathbf{v}_E is the $\mathbf{E} \times \mathbf{B}$ drift velocity, $\mathbf{B} = B \hat{\mathbf{b}}$ is the equilibrium magnetic field, u_{\parallel} is the electron fluid velocity along \mathbf{B} , $\tilde{\nabla}_{\parallel} = \hat{\mathbf{b}} \cdot \nabla - \hat{\mathbf{b}} \times \nabla A_{\parallel} \cdot \nabla$ is the gradient along the total magnetic field, ω_* is the diamagnetic frequency, ω_d is the combined ∇B and curvature drift frequency, A_{\parallel} is the magnetic potential normalized to $\rho_i B$, $\rho_{i,e} = v_{i,e}/\Omega_{i,e}$ is the thermal gyroradius, $\Omega_{i,e}$ is the gyrofrequency, $v_{i,e} = \sqrt{T_{i,e}/m_{i,e}}$ is the thermal speed, $T_{i,e}$ is the equilibrium ion or electron temperature, and $\eta_{i,e}$ is the ratio of density to temperature scale lengths ($\eta_{i,e} = L_n/L_{T_{i,e}}$). Conventional normalizations are used, with equilibrium lengths normalized to the electron density scale length (L_n), and velocities normalized to $c_s = \sqrt{T_e/m_i}$. The lowest order fluctuating electron temperature $T^{(0)}$ is extracted via numerical inversion of the isothermal condition along the field line, $\tilde{\nabla}_{\parallel} (T^{(0)} + T_e) = \tilde{\nabla}_{\parallel} T^{(0)} - \eta_e i\omega_* A_{\parallel} = 0$, which arises from the dominant terms in the higher moment equations. The next order corrections to the temperature, $T_{\parallel}^{(1)}$ and $T_{\perp}^{(1)}$, can also be extracted from the full set of electron moment equations, closed with an appropriate toroidal Landau closure such as that in [4]. In this work, only the parallel Landau damping correction in the momentum

equation, $\tilde{\nabla}_{\parallel} T_{\parallel}^{(1)} \rightarrow \sqrt{\pi/2} v_i/v_e |k_{\parallel}| u_{\parallel}$ is kept. Neglecting this electron Landau damping term (formally taking $m_e/m_i \rightarrow 0$) leads to a model which is isothermal along the field. Numerical simulations are carried out both with and without this term. Electron-ion collisions are modeled by the simple operator $\mathcal{C}_{ei} = \hat{v}_{ei}(u_{\parallel} - u_{\parallel i})$.

This electron model is both simple and practical for implementation in numerical simulations, as it introduces neither the short timescales associated with electron free streaming along the field, nor the small spatial scales associated with the electron gyroradius and skin depth. Furthermore, the model represents a significant improvement over the adiabatic passing electron response used in most past simulations. In addition to finite- β effects and Alfvén wave dynamics, the model incorporates electron $\mathbf{E} \times \mathbf{B}$, curvature and ∇B drift motion, as well as linear electron Landau damping and the dominant $\mathbf{E} \times \mathbf{B}$ and magnetic flutter nonlinearities. Note that the separation of scales assumed in the derivation ($\omega \ll k_{\parallel} v_e$, with Alfvén frequencies allowed) requires that the ratio of electron to magnetic pressure (β_e) far exceed the mass ratio m_e/m_i , a condition nearly always satisfied in the hot core of a fusion-relevant plasma, but which can break down very near the edge. The model is intended to describe only the untrapped electron distribution, and it treats the variation of $|B|$ along the field as a small perturbation ($\nabla_{\parallel} \ln B \sim \sqrt{m_e/m_i}$). Coupling to an appropriate trapped electron model is an important direction for future work.

It will be useful to benchmark results using this electron Landau closure with recently developed, fully kinetic electromagnetic turbulence simulations [16], which may soon be run for the core plasma parameters we consider here. Improved versions of the electron Landau damping model (such as including an integral convolution representation to evaluate the $|k_{\parallel}|$ operator along perturbed field lines [17]) could eventually be tried. In the present form, the full electron model can be viewed as an extension of the work of Kadomtsev and Pogutse [18] to incorporate toroidal drifts, parallel ion flow, and an improved Landau damping model which phase mixes $\mathbf{E} \times \mathbf{B}$ driven perturbations [10]. This electron Landau damping model looks similar to an enhanced resistivity, with an enhancement factor of $\sim 10^2$ for typical core

tokamak parameters.

Ion dynamics are described by an electromagnetic gyrofluid model, though a direct gyrokinetic method could be substituted. The ion equations are derived by taking six moments of the electromagnetic gyrokinetic equation [9,19] employing Landau closure models [4,5,10]. [We use the Landau closures of Ref. [4], and are currently investigating recent neoclassical improvements [1] for the electromagnetic case. The simulations reported here employ the large aspect ratio limit ($r/R \rightarrow 0$) in which neoclassical effects vanish.] The resulting ion equations are similar to Refs. [4,5], with the addition of magnetic induction terms and with $\nabla_{\parallel} \rightarrow \tilde{\nabla}_{\parallel} = \hat{\mathbf{b}} \cdot \nabla - \hat{\mathbf{b}} \times \nabla A_{\parallel} \cdot \nabla$ to include linear and nonlinear magnetic flutter effects. The gyrokinetic Poisson equation [8] and Ampere’s Law [9,19] close the system.

The complete electron and ion “gyrofluid” model has been extensively benchmarked against linear gyrokinetic theory. Figure 1 shows a comparison of linear growth rate (γ) and frequency (ω) spectra of the ITG mode with the GS2 kinetic code [20], using the parameters $\eta_i = \eta_e = 5$, $R/L_n = 3$, $s = 1$, $q = 2$, $m_e/m_i = 0$, and $\tau = T_i/T_e = 1$, where s is the magnetic shear and q is the safety factor. Trapped electrons, not included in the model, are neglected in the benchmark by setting the inverse aspect ratio (r/R) to zero. The comparison is undertaken at three values of $\beta = 0, 0.4, 0.6\%$, with the model successfully reproducing the substantial finite- β stabilization of the ITG mode which occurs below the ideal MHD β limit (0.7% in this case).

The gyrofluid model also reproduces the correct linear behavior of the kinetic ballooning mode (KBM), an instability in the shear Alfvén branch of the dispersion relation driven by the pressure gradient and kinetic effects. Figure 2 shows comparisons with kinetic theory [21], with $R/L_n = 4$, $s = 1$, $q = 2$, $\tau = 1$, and $k_{\theta}\rho_i = 0.5$. Figure 2(a) shows a case with flat temperature profiles ($\eta_i = \eta_e = 0$) where the KBM goes unstable precisely at the ideal MHD ballooning limit. In Fig. 2(b), a finite ion temperature gradient ($\eta_i = 2$) drives the KBM unstable below the ideal ballooning limit due to an ion drift resonance effect [22]. This effect can lead to significant transport below the calculated ideal stability limit, and its accurate description is critical for a complete transport model.

Nonlinear simulations are carried out in a toroidal flux tube geometry [4] using an updated, massively parallel version of the GRYFFIN gyrofluid code. As prior core transport studies have been undertaken in the zero β limit, it is of great interest to explore the functional dependence of transport on β . To this end, a series of six simulations is carried out with fixed profiles ($R/L_n = 3, q = 2, s = 1, \eta_i = \eta_e = 3, \tau = 1$) but varying β from zero to 1%, approaching the ideal ballooning limit of 1.1%. A simple s - α shifted circle equilibrium is used in this study, with the Shafranov shift parameter (α) chosen to be consistent with β , though the code is capable of general equilibrium geometry. At moderate β , the ITG is the linearly dominant mode, though its growth rate decreases steadily with β . The KBM is dominant only in the $\beta = 1\%$ case, though it is unstable at lower β . All simulations employ a 128×96 Fourier space grid in the radial and poloidal directions and 32 real space grid points along the field. Approximately 10^5 time steps of $2 \pm 1 \times 10^{-3} L_n/c_s$ have been evolved in each case. Heat transport is found to be dominated by $\mathbf{E} \times \mathbf{B}$ fluctuations in all cases, with the magnetic flutter term smaller by at least an order of magnitude.

The variation of the time averaged steady-state ion heat conductivity (χ_i) with β , from simulations without electron Landau damping or collisions, is shown in Fig. 3(a). Two simple mixing length estimates, with constants fit to the $\beta = 0$ simulation results, are also shown. Here the nonlinear behavior of the system can be qualitatively understood in terms of linear physics. For $\beta/\beta_c \lesssim 1/2$, the conductivity decreases with β due to the finite β stabilization of the ITG mode. As β approaches β_c , the KBM is becoming unstable and driving an increase in χ_i .

The addition of electron Landau damping (using the electron/deuterium mass ratio) breaks the isothermal electron constraint, and changes the nonlinear behavior of the system dramatically. [A small amount of collisions, ($\hat{\nu}_{ei} = 5 \times 10^{-5}$), was also included in these runs but has little effect.] The linear growth rate spectrum, and hence simple mixing length estimates of χ_i , change only modestly. Yet the steady state χ_i increases by a factor of five at $\beta = 0.8\%$ and by a factor of eight at $\beta = 1.0\%$, as illustrated in Fig. 3(b). In finite- β simulations with electron Landau damping, significant particle and electron heat transport

are also measured. The diffusivity and electron heat conductivity scale similarly to χ_i but are reduced in magnitude by a factor of 3-4.

This large increase in χ_i as the ideal β limit is approached corresponds to a qualitative change in the turbulent dynamics, illustrated by Fig. 4. The eddy turnover time decreases by roughly a factor of four, comparable to the linear difference in frequency between the ITG and KBM at these parameters, and short-lived radially extended streamers appear.

The transition from predominantly electrostatic ion-drift wave turbulence to Alfvénic turbulence can be quantified by the ratio of the mean square parallel electric field ($E_{\parallel} = -\nabla_{\parallel}\phi - \partial A_{\parallel}/\partial t$) to its electrostatic constituent, $\nabla_{\parallel}\phi$, shown in Fig. 5. In the usual model of ion drift wave turbulence, this ratio is taken to be one, and magnetic fluctuations are neglected. In contrast, in “ideal” Alfvénic turbulence, magnetic induction exactly balances $\nabla_{\parallel}\phi$ and the ratio is zero. Figure 5 demonstrates that the electrostatic approximation can break down at modest values of $\beta/\beta_c \sim 1/2$, and that the turbulence becomes predominantly Alfvénic as the ideal ballooning limit is approached. This transition is hindered somewhat by the presence of electron dissipation, which allows force balance to be achieved at large E_{\parallel} , even when $\nabla_{\parallel}n_e$ is small.

Steady state density and temperature fluctuation spectra have been extracted from the simulations and show a number of similarities to fluctuation measurements [23,24]. The radial spectra peak at zero, while the poloidal spectra peak at poloidal wave number $k_{\theta} = 0.20 \pm 0.05 \rho_s^{-1}$, nearly independent of β . The width of the peaks decreases significantly with β , with the FWHM dropping roughly a factor of three as β increases from 0 to 1%. The simulations produce ion temperature spectra nearly identical in shape to the density fluctuation spectra, with a ratio of the relative temperature fluctuations to the relative density fluctuations of 2 ± 0.5 , largely independent of parameters, similar to the measured behavior of carbon fluctuations [24]. Further investigation using the detailed geometry and parameters from the experiment is needed to confirm this agreement.

An important limitation of electrostatic simulations has been their inability to predict the dramatic increase in heat conductivity often seen in the outer $\sim 30\%$ of tokamak plasmas.

The increase in χ_i at moderate $\alpha = -Rq^2\beta' \sim \beta/\beta_c$ seen in electromagnetic simulations is a candidate to explain the observed behavior, because while β itself decreases in the outer regions of tokamak plasmas, α often increases due to sharp gradients and increasing q . A preliminary study using parameters from a TFTR L-mode shot has indeed found that electromagnetic simulations predict much larger fluxes than electrostatic simulations of the outer region, bringing the simulation results into better agreement with measured fluxes. There are also nonlinear instability mechanisms that can be important for edge parameters (Refs. [13,12] and references therein).

In summary, a new method has been developed for the efficient simulation of plasma turbulence, including magnetic fluctuations and non-adiabatic passing electron dynamics. The method has been implemented in realistic three dimensional nonlinear simulations, which exhibit fluctuation spectra with several characteristics in common with measurements [23,24]. A transition from nearly electrostatic ion-drift turbulence to Alfvénic turbulence is observed to occur as β is increased above a threshold value of roughly half the ideal critical β_c . The scaling of heat transport with β has been explored, and ion heat conductivity is found to decrease with β far from the ideal ballooning limit, but to increase with β as the ballooning limit is approached. In the presence of electron Landau damping, this increase in heat transport with beta can be dramatic and can occur well below the ideal ballooning threshold, perhaps helping to explain the high heat conductivity measured in the outer region of many tokamak experiments.

This is a report of work supported by the U.S. Department of Energy under Grant No. DE-FG03-95ER54309, Contract No. DE-AC02-76CH03073, and by an NSF fellowship. The authors thank M.A. Beer and W. Dorland for many useful discussions and for providing the massively parallel, electrostatic toroidal gyrofluid code that was the starting point of our calculations, and thank M. Kotschenreuther for helpful discussions and for the use of his gyrokinetic GS2 code. Computer resources were provided by the National Energy Research Supercomputer Center, and by the Los Alamos Advanced Computing Lab, as part of the computational grand challenge Numerical Tokamak Turbulence Project.

REFERENCES

- [1] A. M. Dimits *et al.*, to appear in Phys. Plasmas (2000).
- [2] S. E. Parker, W. W. Lee, and R. A. Santoro, Phys. Rev. Lett. **71**, 2042 (1993).
- [3] Z. Lin *et al.*, Science **281**, 1835 (1998).
- [4] M. A. Beer and G. W. Hammett, Phys. Plasmas **3**, 4046 (1996). G. W. Hammett, M. A. Beer, W. Dorland, S. C. Cowley, and S. A. Smith, Plasma Phys. Control. Fusion, **35**, 973 (1993).
- [5] R. E. Waltz, G. D. Kerbel, and J. Milovich, Phys. Plasmas **1**, 2229 (1994); R. E. Waltz, G. D. Kerbel, J. Milovich, and G.W. Hammett, Phys. Plasmas **2**, 2408 (1995).
- [6] A. M. Dimits, T. J. Williams, J. A. Byers, and B. I. Cohen, Phys. Rev. Lett. **77**, 71 (1996).
- [7] E. A. Frieman and L. Chen, Phys. Fluids **25**, 502 (1982).
- [8] W. W. Lee, Phys. Fluids **26**, 556 (1983).
- [9] T. S. Hahm, W. W. Lee, and A. Brizard, Phys. Fluids **31**, 1940 (1988).
- [10] G. Hammett and F. Perkins, Phys. Rev. Lett. **64**, 3019 (1990).
- [11] J. Y. Kim, W. Horton, and J. Q. Dong, Phys. Fluids B **5**, 4030 (1993).
- [12] B. N. Rogers and J. F. Drake, Phys. Rev. Lett. **79**, 229 (1997).
- [13] B. Scott, Plasma Phys. Controlled Fusion **39**, 1635 (1997).
- [14] X. Xu and R. Cohen, Contrib. Plasma Phys. **38**, 158 (1998).
- [15] A. Zeiler, J. F. Drake, and B. N. Rogers, Phys. Rev. Lett. **84**, 99 (2000).
- [16] F. Jenko and B. D. Scott, Phys. Plasmas **6**, 2705 (1999); F. Jenko, W. Dorland, M. Kotschenreuther, B.N. Rogers, to appear in Phys. Plasmas (2000).

- [17] P. B. Snyder, G. W. Hammett, and W. Dorland, *Phys. Plasmas* **4**, 3974 (1997).
- [18] B. B. Kadomtsev and O. P. Pogutse, in *Plasma Physics and Controlled Nuclear Fusion Research, 1984* (International Atomic Energy Agency, Vienna, 1985), Vol. 2, p. 69.
- [19] A. Brizard, *Phys. Fluids B* **4**, 1213 (1992).
- [20] M. Kotschenreuther, G. Rewoldt, and W. M. Tang, *Computer Physics Communications* **88**, 128 (1995).
- [21] B.-G. Hong, W. Horton, and D.-I. Choi, *Phys. Fluids B* **1**, 1589 (1989).
- [22] F. Zonca, L. Chen, J. Q. Dong, and R. A. Santoro, *Phys. Plasmas* **6**, 1917 (1999).
- [23] R. J. Fonck *et al.*, *Phys. Rev. Lett.* **70**, 3736 (1993).
- [24] H. T. Evensen *et al.*, *Nucl. Fusion* **38**, 237 (1998).

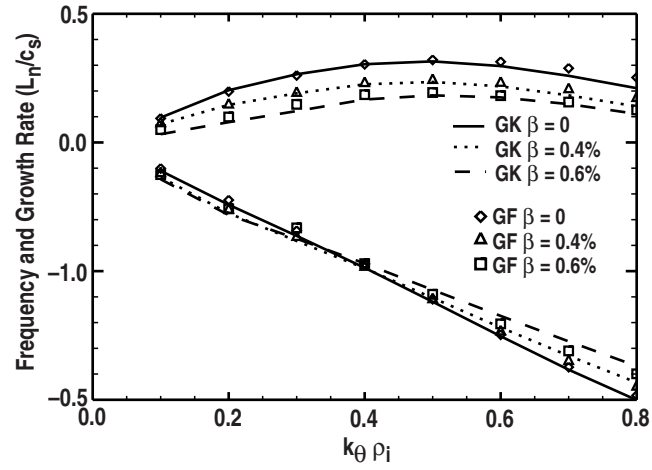


Fig. 1. Linear growth rate (positive) and frequency (negative) spectra of the toroidal ITG mode, for $\beta = 0$, $\beta = 0.4\%$, and $\beta = 0.6\%$. The gyrofluid (GF) result is compared with results from the GS2 linear gyrokinetic code.

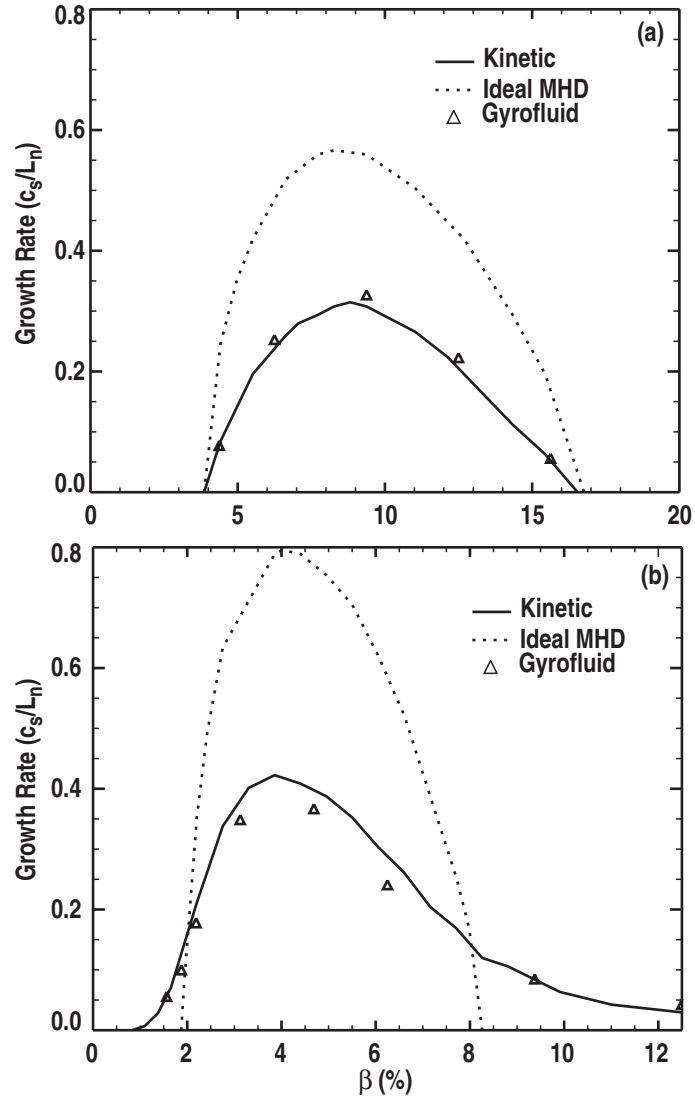


Fig. 2. γ vs. β for the KBM, with (a) $\eta_i = 0$, (b) $\eta_i = 2$.

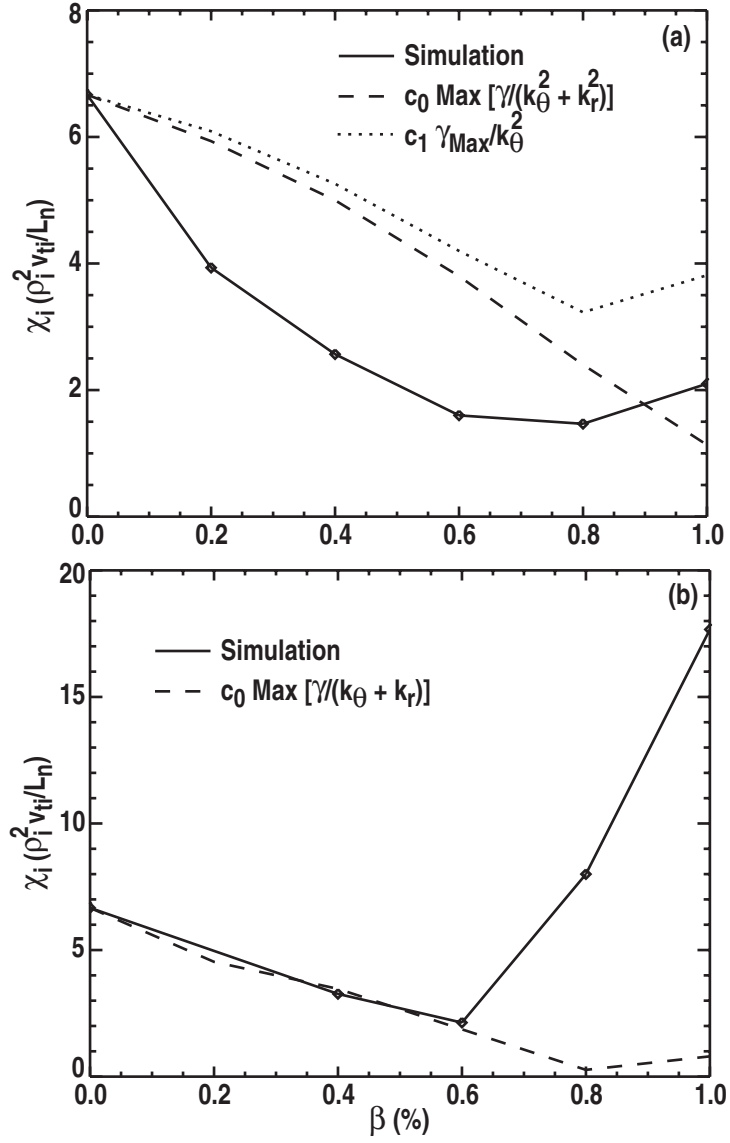


Fig. 3. Ion heat conductivity (χ_i) vs. β (a) without and (b) with electron dissipation.

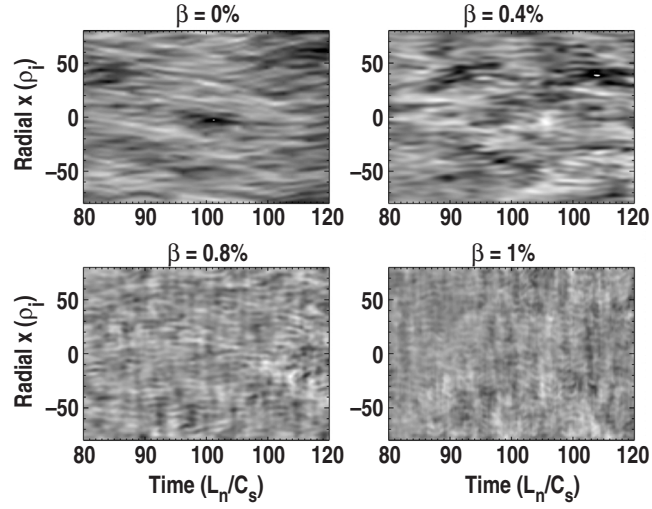


Fig. 4. Contour plots of the electrostatic potential on the outer midplane vs. time and radius, at four values of the plasma β .

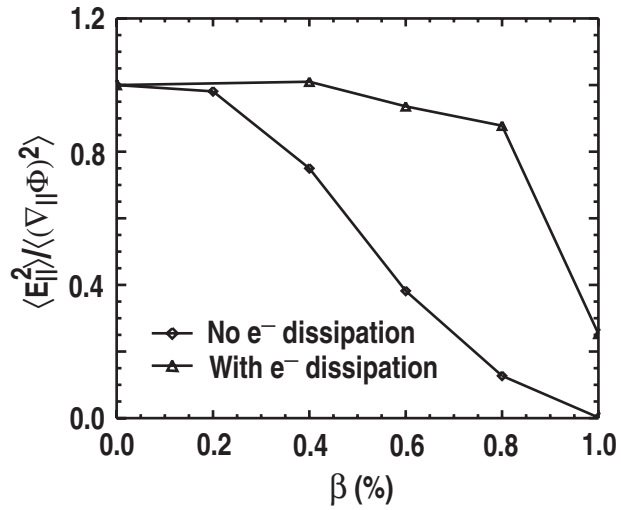


Fig. 5. The mean squared parallel electric field divided by its electrostatic component illustrates the transition from electrostatic to Alfvénic turbulence as β is increased.